Electric Power Systems Research 104 (2013) 183–192

Contents lists available at ScienceDirect

Electric Power Systems Research

journal homepage: www.elsevier.com/locate/epsr

Power system transient stability analysis via the concept of Lyapunov Exponents

D. Prasad Wadduwage [a,*], Christine Qiong Wu [b], U.D. Annakkage [a]

[a] Departement of Electrical and Computer Engineering, University of Manitoba, Winnipeg, MB R3T 5V6, Canada
[b] Department of Mechanical and Manufacturing Engineering, University of Manitoba, Winnipeg, MB R3T 5V6, Canada

ARTICLE INFO

Article history:
Received 22 March 2013
Received in revised form 20 June 2013
Accepted 21 June 2013
Available online 27 July 2013

Keywords:
Transient stability
Lyaounov Exponents
Fault scenario
Fault clearing time

ABSTRACT

Transient stability of an electrical power system refers to the ability of the system to settle at the stable equilibrium point in the post-fault system subsequent to a specific fault scenario. This stability problem can be studied either as a system stability or a structural stability problem. In this paper, the concept of Lyapunov Exponents (LEs) is used to analyze the transient stability of IEEE 3-generator 9-bus and IEEE 16 generator 69 bus benchmark systems. A spectrum of LEs is calculated from the mathematical models and the Largest Lyapunov Exponent (LLE) being negative implies the exponential stability of the post-fault power system. The system stability regions for specific fault scenarios are determined using the invariance property of the LEs from the initial conditions. Furthermore, the structural stability regions in terms of parameters of the pre-fault system dynamic equations are also determined. This study demonstrates that the concept of LEs can be used as a novel method to determine if the post-fault power system is within the stability region of attraction of the new stable equilibrium point, and hence to determine the stability region. It is also proposed that the largest average exponential rate calculated over a short time window is a sound approach for early prediction of the stability.

1. Introduction

Ensuring stability of a power system is a mandatory requirement to secure the electricity supply to customers. For the purpose of transient stability analysis, a power system is represented by a combination of first order differential equations and algebraic equations. The differential equations describe the dynamic behavior of devices such as generators, controllers and dynamic loads connected at various locations of the system, whereas the algebraic equations describe the network power flow and the current injections from the dynamic devices [1]. This is known as the Differential Algebraic Equation (DAE) representation of the power system. The algebraic equations are the results of ignoring dynamics associated with the network and the stator windings.

In general, a power system operates at a steady-state with all system variables within their desired limits. For given generator outputs and loading situations, this operating point can be considered as a pre-fault stable equilibrium point. Therefore, all the nearby trajectories in the state-space converge to this stable attractor. The smooth operation of the system can be perturbed due to the occurrence of various disturbances which are inevitable. An event-type disturbance is characterized by a specific fault scenario such as a three-phase short circuit of a transmission line in the network followed by a disconnection of the line [2]. Subsequent to an event-type disturbance, if an outage of a power system element occurs, the post-fault system topology changes from that of the pre-fault system. Again, for given generator outputs and loading conditions, the steady-state behavior of the post-fault system must be studied with respect to its stability of the new equilibrium point. If the system is still stable subsequent to the fault scenario, the resulting trajectories in the state-space converge to the stable attractor of the post-fault system. Generator rotor angles are the physical variables of interest during the transient stability analysis of the power system. For given generator outputs and loading situations the transient stability problem can be studied in two ways: (a) stability of the post-fault system subsequent to the specific fault clearing time, and (b) maximum allowable fault clearing time (i.e. the Critical Clearing Time (CCT)) for which the subsequent system response remains stable [2]. A change in fault clearing time results in a change in initial values of the state variables of the post-fault system dynamic equations. Therefore, for given generator outputs/load combinations of the pre-fault and post-fault network, the transient stability of the system depends only on the post-fault system initial conditions, which in turn depends on the fault clearing time. From a theoretical viewpoint of system stability, this scenario relates to the *system stability* where the disturbance is imposed on the initial conditions and the CCT represents the

* Corresponding author. Tel.: +1 204 474 8873.
E-mail addresses: umwadduw@cc.umanitoba.ca, prasad@elect.mrt.ac.lk (D.P. Wadduwage).

0378-7796/$ – see front matter.
http://dx.doi.org/10.1016/j.epsr.2013.06.011

boundary of the stability region. On the other hand, the load of the customers change with time during the operation of an actual power system and the generator outputs are adjusted to cater for this changing demand. The adjustments of generator power outputs can be interpreted as changes in the parameters of the power system dynamic equations. Therefore, even for a fixed fault clearing time of the same fault scenario, changes in dynamic equation parameters vary the initial conditions of the post-fault system. The interest in this case is the continuous region enclosed by the parameters (the generator power outputs) so that the post-fault system remains stable subsequent to the fault scenario with a known fault clearing time. From Lyapunov's stability viewpoint, this scenario relates to the *structural stability* where the disturbance is imposed on the parameters of the dynamic equations. Overall, considering the above two scenarios the transient stability problem can be treated either as a *system stability* problem or a *structural stability* problem.

Traditionally the power system transient stability is determined using Time Domain Simulation (TDS) approach [1–3]. The DAEs of the system during pre-fault, during-fault, and post-fault situations are numerically solved to determine the time domain trajectories of the variables. The system is said to be transiently stable if the TDS trajectories converge to the exponentially stable equilibrium point of the post-fault system. Power utilities perform TDS using commercial software to determine the system behavior and is treated as the benchmark when assessing transient stability.

Furthermore, Machine Learning (ML) methods have also gained interest among power system researchers as suitable tools for predicting the transient stability of the power system. Artificial Neural Networks (ANN), Fuzzy systems, Decision Trees (DT) and Support Vector Machines (SVM) have been widely studied in this regard [4–8]. In this approach a database is created for a given network by considering possible conditions and a classifier is trained by using one of the ML techniques. Thereafter, this classifier is used to determine the system stability during any operating condition. These machine-learning-methods based techniques accurately predict the system stability provided that the classifiers have been trained extensively for possible conditions. However, a limitation of this approach is that the classifier performance depends entirely on the network configuration.

The power system transient stability problem can be analyzed using the Lyapunov's stability theory in that it involves studying whether the trajectories in a region surrounding the post-fault equilibrium point converge or diverge. The stability of the system can be determined by constructing a positive-definite Lyapunov function, which decreases monotonically along the system trajectory [9]. Literature on power systems has discussed the applications of Lyapunov's second method to predict the transient stability, and the candidate Lyapunov functions have been based on kinetic and potential energies of the system [10–13]. The main advantage of using Lyapunov's stability theory is that a Lyapunov function is an invariant property to the nonlinear systems, i.e., the conclusion of the system stability is independent from the initial conditions within the stability regions. However, the lack of a constructive method for deriving a Lyapunov function limits the applications of this otherwise powerful approach for nonlinear systems.

The concept of LEs is another powerful tool in analysing the stability of nonlinear dynamic systems. The LEs are the average exponential rates of divergence or convergence of nearby trajectories in the state-space [14,15]. They provide qualitative and quantitative characteristics of the system dynamics. Generally the sum of all the LEs represents the average volume contraction/expansion rate in the state-space, and the signs of LEs indicate the asymptotic property of the dynamical system. Furthermore, the LEs are invariant from the initial conditions within the same stability region [16]. The most attractive advantage of the concept of LEs is that the methods for calculating the exponents are constructive, making the stability analysis of complex dynamical systems possible. The concept of LEs has been applied to the analysis of the asymptotically stable equilibrium point of the post-fault power systems in [17] and [18]. In [18], a phasor measurement unit-based online monitoring algorithm was proposed for rotor angle stability of power systems. LEs were used to estimate the system stability. The work has two limitations; (1) the LEs were calculated over a short time interval, and the convergence of the exponents is in question, and (2) an essential part of stability analysis is to determine the stability region, which was not addressed in the previous work [18]. Furthermore, determination of the stability region of a transiently stable power system in terms of the pre-fault system operating parameters is important since it provides the information regarding the security of the current operating point. The power system literature suggests different approaches for transient stability boundary determination [8,19] as well as triggering preventive and corrective actions if the system is outside the secure region [20]. These methods have been focused on the speedy prediction of the system stability accommodating the increased complexity of the system. On the other hand, the concept of LEs seems to play a key role in stability region determination since the exponents are invariant from initial conditions within the same stability region [16]. This invariance property of the exponents has been used during this study.

The objective of this paper is to conduct a systematic stability analysis of the power systems using the concept of LEs. Such an analysis consists of (1) determining the power system transient stability, (2) determining the system stability region and hence the CCT of the system under a given fault scenario, and (3) performing a comprehensive structural stability analysis of the power system. This study uses the IEEE 3-generator 9-bus test system [3] and IEEE 16 generator 69 bus test system [25] to demonstrate the idea.

Table 1
Steady-state generator data on 100 MVA base.

Generator no	Terminal voltage magnitude (pu)	Real power output (pu)
Gen 1 (Swing Gen)	1.040	0.716
Gen 2	1.025	1.630
Gen 3	1.025	0.850

Table 2
Generator dynamic data.

Generator no	H (s)	D/M*
Gen 1	23.64	0.1
Gen 2	6.40	0.2
Gen 3	3.01	0.3

* $M = \frac{2H}{\omega_0}$, where ω_0 is the synchronous speed [3].

2. Methodology

2.1. Problem formulation

The IEEE 3 generator 9 bus test system [3] consists of three generators with nine buses feeding three loads connected to the load buses 5, 6 and 8 as shown in Fig. 1. The system is initially operating at its stable pre-fault equilibrium point. The generator terminal voltage magnitudes and the real power outputs at this steady operating point are given in Table 1 and the generator dynamic data are given in Table 2. The per unit power consumptions on 100 MVA base of the loads connected to the buses 5, 6 and 8 at the steady operating point are $1.25 + j0.5$, $0.9 + j0.3$, and $1 + j0.35$ respectively [3]. The generator was modeled using the classical generator model

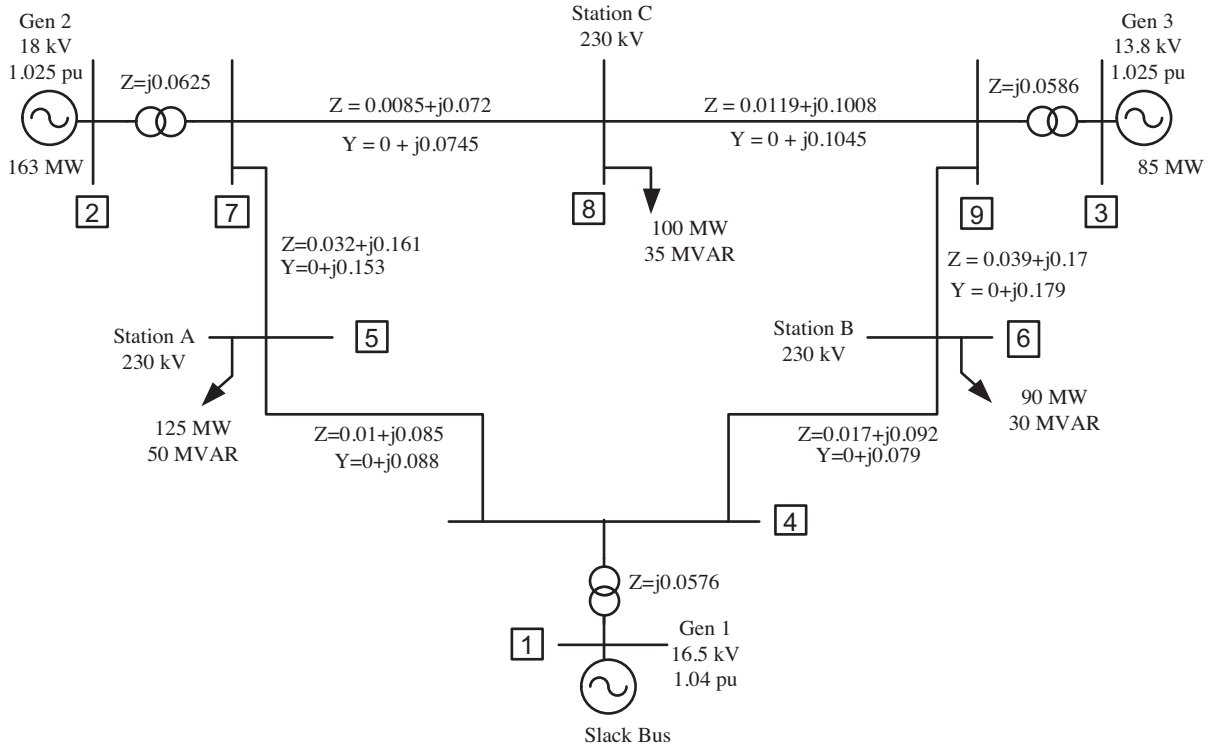

Fig. 1. IEEE 3-generator 9-bus test system.

[1] with a voltage source of constant magnitude behind its transient reactance. The three loads were modeled as constant admittances connected in shunt at the respective bus bars and the bus 1 was considered as an infinite bus.

The dynamic behavior of a generator is given by Eq. (1).

$$\frac{2H}{\omega_0}\frac{d^2\delta}{dt^2} = \bar{T_m} - \bar{T_e} - \frac{K_D}{\omega_0}\frac{d\delta}{dt} \tag{1}$$

where ω_0 is the synchronous speed, $\bar{T_m}$ is the input mechanical torque of the generator in pu, and $\bar{T_e}$ is the generator air gap torque output in pu.

Eq. (1) can be expressed as two first order differential equations;

$$\begin{aligned}\frac{1}{\omega_0}\frac{d}{dt}\delta &= \Delta\omega \\ \frac{d}{dt}\Delta\omega &= \frac{1}{2H}\left(\bar{T_m} - \bar{T_e} - K_D\Delta\omega\right)\end{aligned} \tag{2}$$

where δ and $\Delta\omega$ represent the angle of the generator internal voltage in radians and the pu generator speed deviation from the synchronous speed respectively.

When the generator is operating around the pre-fault equilibrium point, $\bar{T_m} = \bar{T_e}$. $\bar{T_m}$ was kept constant throughout the simulation and $\bar{T_e}$ was determined using Eq. (3) approximating the rotor speed to be 1.0 pu.

$$T_{ei} = \left|E_i'\right|^2 G_{ii} + \left|E_i'\right| \sum_{j=1, j\neq i}^{n} \left|E_j'\right| \left|Y_{ij}\right| \cos\left(\delta_{ij} - \theta_{ij}\right) \tag{3}$$

where $E_i' = \left|E_i'\right| \angle\delta_i$ is the generator internal voltage, $Y_{ij} = G_{ij} + jB_{ij} = \left|Y_{ij}\right| \angle\theta_{ij}$ is the equivalent admittance between the ith and jth generators, and n is the number of generators in the network.

Combining Eqs. (2) and (3), the dynamic behavior of the ith generator can be represented by two first order differential equations as given in Eq. (4).

$$\begin{aligned}\dot{\delta}_i &= \omega_0\Delta\omega_i \\ \dot{\Delta\omega}_i &= \frac{T_{mi}}{2H_i} - \frac{\left|E_i'\right|^2 G_{ii}}{2H_i} - \frac{\left|E_i'\right|}{2H_i}\sum_{\substack{j=1 \\ j\neq i}}^{n} \left|E_j'\right| \left|Y_{ij}\right| \cos\left(\delta_{ij} - \theta_{ij}\right) - \frac{K_{Di}}{2H_i}\Delta\omega_i\end{aligned} \tag{4}$$

Expanding Eq. (4), the state-space model of the test system can be represented by four first order differential equations since the bus 1 has been considered as an infinite bus. $\left|Y_{ij}\right| \angle\theta$ values in Eq. (4) change depending on the pre-fault, during-fault and post-fault network configuration. The pre-fault equilibrium point $\left(\delta_{2,pre}, \Delta\omega_{2,pre}, \delta_{3,pre}, \Delta\omega_{3,pre}\right)$ is obtained by equating the state-space equations to zero. Assuming that the system operating at steady-state subjects to a specified fault scenario, the resulting dynamic equations during the faulted period are integrated and the values of the state variables $\left(\delta_{2,d}, \Delta\omega_{2,d}, \delta_{3,d}, \Delta\omega_{3,d}\right)$ at the fault clearing time are determined. Hence, $\left(\delta_{2,d}, \Delta\omega_{2,d}, \delta_{3,d}, \Delta\omega_{3,d}\right)$ become the initial conditions of the post-fault system dynamic equations as well as the initial conditions for the LE estimation of the post-fault system. This procedure is illustrated in Fig. 2.

When the post-fault system is transiently stable, the resulting trajectories converge to the stable equilibrium point of the post-fault system. Otherwise, the time domain simulation trajectories would diverge from the equilibrium point of the post-fault system with the simulation time span. However, if such a situation arises, the power system protection identifies it and trips the respective generators from the system. In this present study, the protection devices were not modeled. However, the constraint given in Eq. (5) was used as a screening tool [21], i.e., any scenario which gives the maximum angle difference between any two generators in the

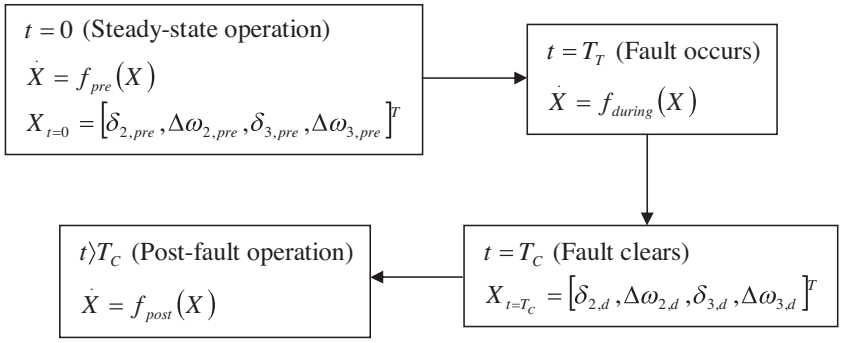

Fig. 2. Dynamic simulation of a power system operating at steady-state, during fault and post-fault.

system at any time greater than or equal to 2π rad, were considered as unstable, and were discarded from further analysis using LEs.

$$\eta_{ij} = \max(\delta_i - \delta_j) \tag{5}$$

where δ_i and δ_j represent the angles of the generators i and j respectively.

2.2. Lyapunov Exponents

The power system is an example of a constrained dynamical system where the state trajectories are limited to a particular subset in the state-space [2]. The concept of LEs has proven to be a constructive tool in analysing the stability of deterministic nonlinear dynamical systems. This concept is based on the fundamental assumption that the nearby trajectories in the state-space evolve exponentially [15]. Thus, the LEs measure the exponential rates of divergence or convergence of nearby trajectories in the state-space. Consider an n-dimensional nonlinear system given by Eq. (6) with $x \in R^n$, $x(0) = x_0$ and $f(x, t)$ is a continuous and differential vector function.

$$\dot{x} = f(x, t) \tag{6}$$

The number of LEs is the same as the dimension of the state-space of the nonlinear system, and are derived based on the long-term evolution of the axes of an infinitesimal n-sphere of initial conditions. Upon its evolution, this infinitesimal n-sphere becomes an n-ellipsoid due to the local deforming nature of the flow. Fig. 3 shows the deformation of the principal axes of the circle and its deformation along the reference trajectory of a 2-dimensional flow. Here, it has been assumed that the initial orthogonal principal axes remain orthogonal after time 't'. However, this assumption is not valid under practical circumstances and

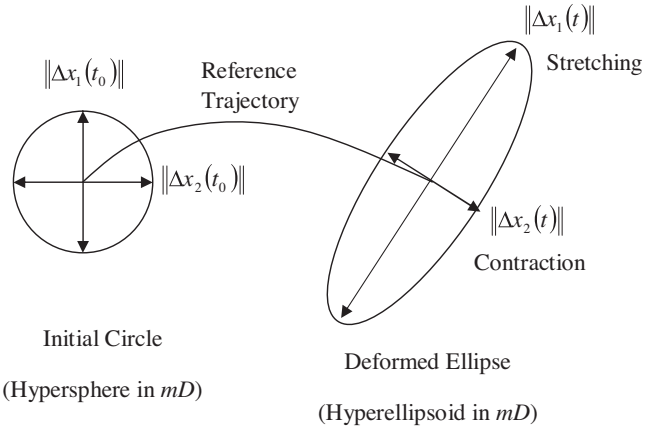

Fig. 3. Evolution of an initially infinitesimal 2D circle along the reference trajectory.

Gram-Schmidt Re-orthonormalization (GSR) should be applied as discussed later. The ith one dimensional LE is then defined in terms of the length of the ellipsoidal principal axes as;

$$\lambda_i = \lim_{t\to\infty} \frac{1}{t} \ln \frac{\|\Delta x_i(t)\|}{\|\Delta x_i(t_0)\|}, \quad i = 1, 2, \cdots, n \tag{7}$$

where $\|\Delta x_i(t)\|$ and $\|\Delta x_i(t_0)\|$ represent the lengths of the ith principal axes at the current time and the initial time respectively. The existence of the above limit is known by Oseledec multiplicative ergodic theorem [22]. However, in practical calculations, the finite time LEs are defined by Eq. (8).

$$\lambda_i = \frac{1}{t} \ln \frac{\|\Delta x_i(t)\|}{\|\Delta x_i(t_0)\|}, \quad i = 1, 2, \cdots, n \tag{8}$$

In the limit as $t \to \infty$, the finite time LEs converges to true LEs of the system.

The LEs are related to the contraction and expansion of different directions in the state-space. However, an exact direction associated with a given exponent cannot be defined since the orientation of the ellipsoid changes continuously as it evolves. A negative exponent reflects an axis which is contracting on average.

Estimation of LEs from a mathematical model has been well established. Different authors have proposed different algorithms on this regard [14,23,24]. Wolf et al. [14] pioneered the work and developed the 'standard algorithm' for LE estimation from mathematical models. During the calculation procedure, the reference trajectory of an n-dimensional continuous time system is determined by the action of the nonlinear equations of motion on an initial condition. The nearby trajectories are defined by evolution of the principal axes of n-hypersphere via the linearized equations of motion. This gives rise to the simultaneous solution of the following set of equations;

$$\begin{Bmatrix} \dot{x} \\ \dot{\varphi}_t \end{Bmatrix} = \begin{Bmatrix} f(x) \\ J\varphi_t \end{Bmatrix} \tag{9}$$

where $x(t) = [x_1(t)x_2(t)\ldots, x_n(t)]$ is a vector of state variables of the differential equations, φ_t is the state transition matrix of the linearized system; $\Delta x(t) = \varphi_t \Delta x(0)$ and J is the $n \times n$ Jacobean matrix determined as;

$$J_{ij} = \left.\frac{\partial f_i}{\partial x_j}\right|_{x=x(t)} \tag{10}$$

The initial conditions of the above system are $x(t_0) = x_0$ and $\varphi(t_0) = I$ where, 'I' represents the identity matrix.

During the above integration, the principal axes of the initial n-hypersphere would tend to fall along the direction of the most rapid growth. In order to avoid this misalignment of vectors, the resulting vectors from the tangent space integration, $\Delta x_1, \Delta x_2, \cdots,$

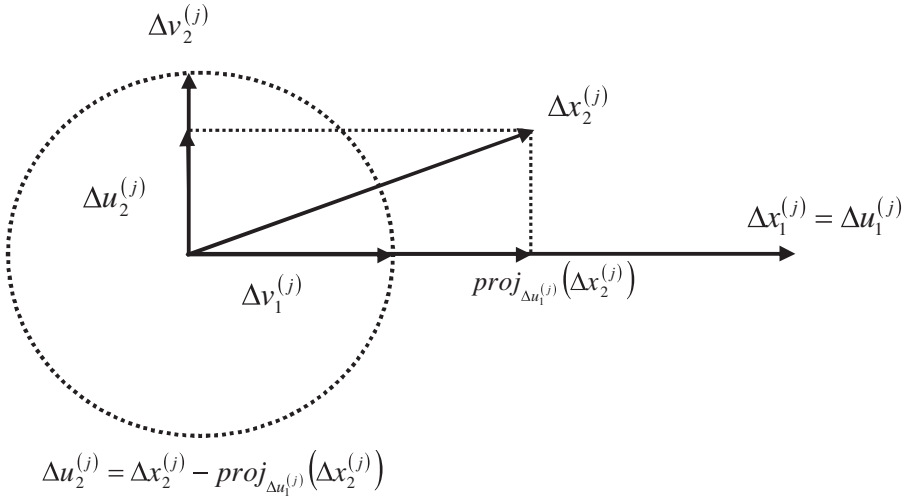

Fig. 4. Geometrical interpretation of GSR of two principal axes $\Delta x_1^{(j)}$ and $\Delta x_2^{(j)}$ at jth integration step.

Δx_n are processed using GSR at each integration time step. The GSR first results in a set of orthogonalized vectors, $\Delta u_1, \Delta u_2, \cdots, \Delta u_n$ and then a set of orthonormalized vectors, $\Delta v_1, \Delta v_2, \cdots, \Delta v_n$ as determined by Eq. (11), where $\langle\rangle$ represents the inner product of vectors.

$$\begin{aligned}
&\Delta u_1 = \Delta x_1, \qquad \Delta v_1 = \frac{\Delta u_1}{\left\|\Delta u_1\right\|}\\
&\Delta u_2 = \Delta x_2 - \left\langle \Delta x_2, \Delta v_1 \right\rangle \Delta v_1, \qquad \Delta v_2 = \frac{\Delta u_2}{\left\|\Delta u_2\right\|}\\
&\vdots\\
&\Delta u_n = \Delta x_n - \left\langle \Delta x_n, \Delta v_{n-1} \right\rangle \Delta v_{n-1} - \cdots - \left\langle \Delta x_n, \Delta v_1 \right\rangle \Delta v_1, \quad \Delta v_n = \frac{\Delta u_n}{\left\|\Delta u_n\right\|}
\end{aligned} \tag{11}$$

Fig. 4 shows the geometrical interpretation of the orthonormalization of two principal axes Δx_1 and Δx_2 at the jth time step. Assuming Δx_1 is the base vector (Δu_1) for the orthonormalization procedure, Δx_2 is first orthogonalized with respect to Δx_1 which gives the vector Δu_2. The two vectors Δu_1 and Δu_2 are then normalized to have the unity magnitudes where these two vectors, Δv_1 and Δv_2 become the initial conditions of the dynamic equations which determine the evolution of principal axes during the next time step.

Once the orthogonal vector frame $\Delta u_1, \Delta u_2, \cdots, \Delta u_n$ is available by GSR, for a sufficiently large integer k, the ith LE can be estimated using Eq. (12).

$$\lambda_i \approx \frac{1}{kh}\sum_{j=1}^{k} \ln \left\| \Delta u_i^{(j)} \right\|, \quad i = 1, 2, \cdots, n \tag{12}$$

where h is the integration time step.

According to the above procedure, it is observed that this computation involves simultaneous solution of $n(n+1)$ number of equations, n equations for the reference trajectory and n copies of tangent map equations.

3. Results of stability analysis

3.1. System stability subsequent to a specified fault scenario with a known fault clearing time

This section discusses the stability of the test system, shown in Fig. 1, subsequent to a clearing of a specified fault scenario after a known fault clearing time. The fault scenario considered here was a three-phase solid fault in the line 8–9, very close to the bus bar 8 and was cleared after four cycles of the fundamental frequency (60 Hz) by disconnecting the faulted line from the network. The LE estimation algorithm was implemented in MATLAB in the PC environment. The dynamic equations described in Eq. (4) were numerically integrated using RK-2 method with a time step of 1/120 s, which is a standard time step used during TDS. The exponent estimation was started using the state values at the fault clearing time. Table 3 shows the estimated LEs up to the 5th decimal place.

Accordingly, all the four LEs are negative. This implies that the trajectories converge to an exponentially stable equilibrium point. Further, the system is transiently stable under the given fault scenario for the considered fault clearing time. Therefore, for the given generator outputs/load combinations, the stability of the IEEE 3-generator 9-bus test system shown in Fig. 1 without the line connecting the bus bars 8 and 9 is uniquely characterized by the four LE values shown in Table 3. Fig. 5 shows the variation of LLE with time. The behavior of the LLE up to 30 s is zoomed in this figure. As can be seen, initially the LLE value fluctuates drastically. Conceptually, the convergence of the LEs is of utmost importance to conclude the exponential stability of the system. Therefore, deciding the power system transient stability based on the exponents calculated over a short time interval as proposed in [18] is not recommended. Fig. 5 shows that the LLE has to be calculated over a sufficiently long time until it converges to the value shown in Table 3.

Fig. 6 shows the TDS trajectories of the state variables under the above scenario. Since the post-fault system is stable subsequent to a disturbance, the resulting trajectories converge to the stable

Table 3
LEs after 500 s.

Lyapunov Exponents (LEs)	1st LE	2nd LE	3rd LE	4th LE
Numerical value	−0.10122	−0.11135	−0.13984	−0.14685

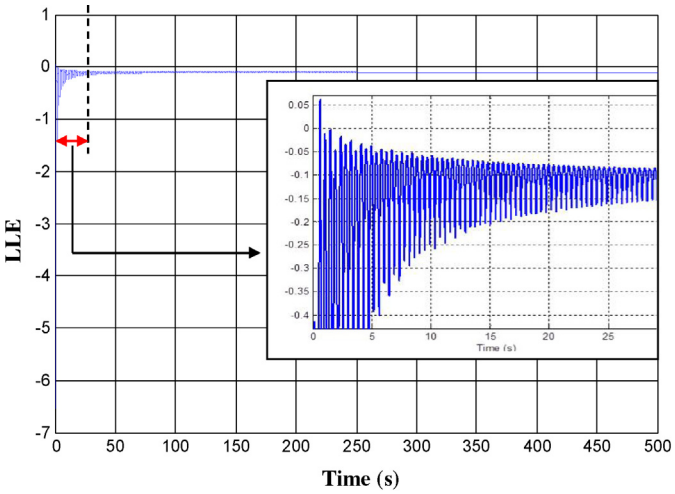

Fig. 5. Time evolution of LLE.

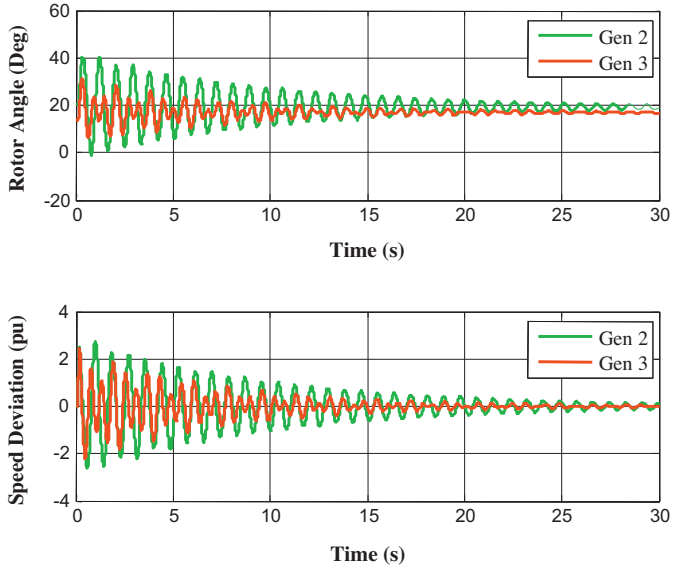

Fig. 6. Evolution of state trajectories.

equilibrium point of the post-fault system exhibiting exponentially damped sinusoidal oscillations.

3.2. Effect of post-fault system topology on the LLE

A power system can subject to different faults anywhere in the system. Faults can occur at different locations leading to outages of different elements of the network. Hence, the post-fault network topology may change subsequent to different fault scenarios. Therefore, the purpose of this section is to investigate the behavior of the LLE with the system topology change.

First, a series of solid three-phase bus faults were applied at different bus bars of the test system and cleared after a predefined period of four cycles of the fundamental frequency (60 Hz) without disconnecting any lines from the network. Since the network topology doesn't change during these cases, the steady-state stable attractors of the pre-fault and post-fault systems remain the same. However, depending on the location of the bus fault, the system dynamic equations during the fault situation change which in turn give different initial conditions for the post-fault system dynamic equations even for the same fault clearing time. The calculated LLE values for this situation are given in Table 4.

Table 4
Variation of LLE with faults at different locations without system topological changes.

Scenario no	Faulted bus	LLE
1	4	−0.108456
2	5	−0.108456
3	6	−0.108455
4	7	−0.108457
5	8	−0.108456
6	9	−0.108456

Table 5
Variation of LLE with system structure.

Scenario no	Faulted bus	Line disconnected	LLE
1	4	Line 4–5	−0.10736
2	4	Line 4–6	−0.11610
3	7	Line 7–5	−0.10800
4	7	Line 7–8	−0.10094
5	9	Line 9–6	−0.10000
6	9	Line 9–8	−0.10138

The estimated LLE values are all negative and identical up to the 5th decimal place irrespective of the fault location. Therefore, the system is stable for the given clearing time irrespective of the fault location. Further, the occurrence of the equal LLE values under all these cases is to be expected since the trajectories converge to the unique stable equilibrium point of the post-fault system irrespective of the fault location. Since the network topology remains unchanged irrespective of the fault location, these results highlight that if a given power system is stable subsequent to a fault scenario without any topological changes, it can be completely characterized by a unique LLE value.

Next, a series of fault scenarios were considered by applying three-phase solid faults on transmission lines near the bus bars (e.g., bus bar 4, 7, 9) in Fig. 1 followed by disconnecting the respective transmission lines (e.g., line 4–5, line 4–6, line 7–5, etc.) from the network after a period of 4 cycles of the fundamental frequency (60 Hz). Since the fault is applied at different locations of the network, the dynamic behavior of the system during the fault changes which in turn results in different values of the state variables at the time of clearing the fault even for the same fault clearing time. Correspondingly, the initial conditions of the LE estimation change for each post-fault network topology. The estimated LLE values up to the 5th decimal during these scenarios are shown in Table 5.

For the considered clearing time, all the LLE values shown in Table 5 are negative confirming that the trajectories are converging toward an exponentially stable equilibrium point. Depending on the disconnecting line, the network power flow changes which in turn results in a different stable attractor for the post-fault system trajectories. Each different, negative LLE value uniquely identifies these stable attractors of different post-fault system topologies.

3.3. System stability region and CCT

During the design process of a power system it is important to determine the maximum possible fault clearing time or the CCT for a given fault scenario for which the subsequent system response remains stable. The transient stability of the post-fault system depends on the values of the state variables at which the fault is cleared. Further, for a given post-fault system topology, these state values change with fault clearing time. Therefore, the stability of the post-fault system can be entirely described as a function of the fault clearing time. If the fault is cleared before the CCT, the subsequent system response remains stable. Hence, the determination of the CCT of a given fault scenario is equivalent to determining the boundary of the stability region of the post-fault system. The

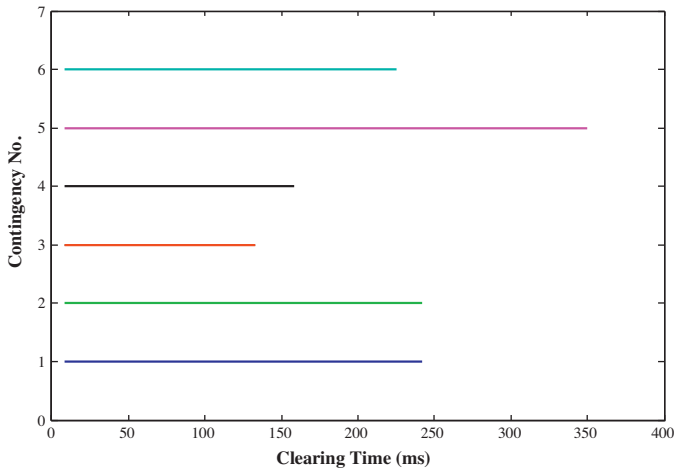

Fig. 7. System stability regions as functions of fault clearing times for different scenarios.

invariance property of the LEs from the initial conditions can be used to determine the stability region of a given system.

In order to determine the stability region using the concept of LEs for each fault scenario, the exponents were calculated by changing the fault clearing times until the constraint given in Eq. (7) is violated. The scenarios considered were the same as mentioned in Table 5. Fig. 7 shows the estimated stability regions for each fault scenario as functions of the fault clearing times. By observing these stability regions, it is possible to determine the severity of the fault scenario in terms of the CCT. For example, the fault scenario 3 has the highest severity since it requires the shortest clearing time, and the severity of the above fault scenarios can be ranked as scenario 3 > scenario 4 > scenario 6 > scenario 2 = scenario 1 > scenario 5. Further, this highlights that the concept of LEs can be used as a constructive tool to determine the boundary of a stability region of a power system.

3.4. Structural stability analysis due to generator outputs/load changes in a power system

The sum of the electrical power outputs of the generators remain equal to the sum of the load demanded by the customers and the system losses during the steady-state operation of the power system. Further, the input mechanical torque and the output electromagnetic torque remain equal at the steady operating point. T_{m2} and T_{m3} are the steady-state mechanical torques of the generators 2 and 3 under various steady-state load conditions. Therefore, changes in T_{m2} and T_{m3} generate distinct steady-state operating points in a two dimensional space. The purpose of this part of the study is to determine the region in the two dimensional space determined by T_{m2} and T_{m3} so that the post-fault system is transient stable subsequent to a known contingency. Here the structural stability analysis is carried out because the disturbance is imposed on the system parameters.

The fault scenario considered was a clearing of a three-phase solid fault in the line 6–9, very close to the bus bar 6, of Fig. 1 after a specific period (4 cycles of the fundamental frequency of 60 Hz) by isolating the faulted line from the network. The study was performed for a set of discrete values of T_{m2} and T_{m3}. For each pair of T_{m2} and T_{m3}, the pre-fault steady-state equilibrium point was determined by equating the dynamic equations given in Eq. (4) to zero. Further, T_{m2} and T_{m3} were kept as constants at the adjusted settings during the simulation. Even for the same fault scenario with a fixed fault clearing time, change in T_{m2} and T_{m3} changes values of the state variables at the fault clearing time, which changes the initial conditions for the LE estimation. The LEs were calculated and T_{m2} and T_{m3} were changed in steps until the constraint given in Eq. (7) is violated. The red curve in Fig. 8 shows the structural stability region in two-dimensional plane determined by T_{m2} and T_{m3} for the considered fault clearing time. The boundary of the stability region is accurate up to ±0.01 pu.

The sensitivity of the stability region with respect to the fault clearing time was determined by repeating the study with fault clearing times of 2, 3, 4, 5, and 6 cycles. The results are shown in Fig. 8. The area covered by the structural stability region reduces with the increase in clearing time. The increase in clearing time for a given T_{m2} and T_{m3} shifts the initial conditions of the post-fault system dynamic equations toward the boundary of its system stability region (i.e. the corresponding stability region determined as a function of clearing time).

The attractiveness of the structural stability regions is that those are determined in terms of pre-fault operating parameters and hence the operator can judge whether the system is operating inside the stability boundary or not and if such a disturbance occurs, the system can lose the stability or not.

4. Faster identification of system stability using the concept of LEs

This section proposes a modified algorithm based on the concept of LEs to systematically derive the stability conclusion which reduces the computational burden associated with the exponent calculation. As presented in Section 3, the LEs need long computing time for the convergence mainly due to the presence of exponentially damped sinusoidal oscillations in a stable post-fault power system. After the convergence of the trajectories, the stability conclusion can be derived by looking at the signs of the exponents. Nevertheless, the magnitudes of the exponents do not provide additional information except the average exponential rate of convergence of the trajectories. Therefore, if the final sign of the LLE can be predicted sooner, the computational burden could be reduced. With this idea in mind, the following revised approach was tested.

Instead of capturing the data from the time of fault clearance (T_C) until convergence, in this modified approach the data are captured after a delay from T_C. Further, instead of computing till convergence the data are collected only up to 5 s from T_C. This will significantly reduce the computing time. The rationale behind the delayed start is to eliminate any highly damped oscillations as its presence at the beginning of the computations make the convergence time longer. The rationale behind early truncation is that we are not interested in the exact value of the LLE as explained in the previous section. We are only interested in whether the LLE is negative or positive.

The performance of the modified algorithm was first tested for the 3 generator 9 bus test system subsequent to clearing the 3-phase solid bus faults applied at different bus bars in the system after 4 cycles of 60 Hz frequency. These contingencies were selected so that the post-fault system remains stable. The system trajectories converge to the unique stable equilibrium point of the post-fault system since the topology remains unchanged. The results are presented in Table 6. The expected negative signs for the stable cases are correctly reflected from the largest average exponential rates calculated over $(T_C - T_C + 5)$ s data window. Results show that the sign of the LLE can be accurately predicted by using a shorter window, thus reducing the computing time.

The performance of the modified algorithm was further tested with the 16 generator 69 bus test system [25] shown in Fig. 9. Due to the space limitations, the steady-state data of the test system are not mentioned and are available in pages 171–175 of [25]. All the generators of the system were modeled using the 6th order

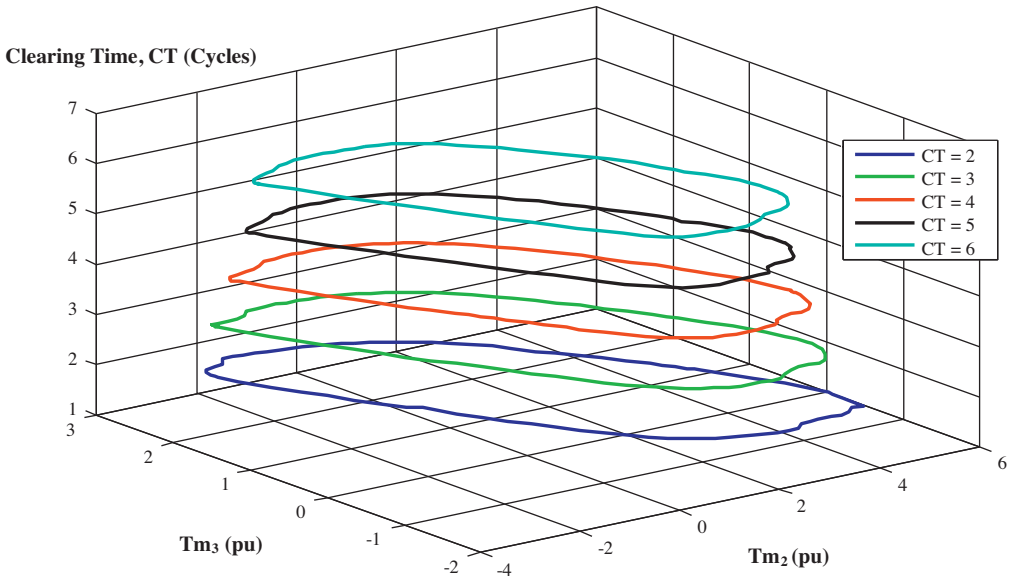

Fig. 8. Change in stability region with fault clearing time.

Table 6
Largest average exponential rates of 3 generator 9 bus system.

Faulted bus	Largest average exponential rates over different time windows				
	$(T_C)-(T_C+5)$ s	$(T_C+0.5)-(T_C+5)$ s	$(T_C+1)-(T_C+5)$ s	$(T_C+1.5)-(T_C+5)$ s	$(T_C+2)-(T_C+5)$ s
4	−0.3413	−0.2202	−0.0713	−0.2165	−0.3138
5	−0.3222	−0.2573	−0.0752	−0.1782	−0.3002
6	−0.3036	−0.2628	−0.0765	−0.1641	−0.2703
7	−0.1316	−0.1673	−0.0619	−0.2718	−0.3116
8	−0.3097	−0.2149	−0.0707	−0.2254	−0.3288
9	−0.3704	−0.1837	−0.065	−0.2364	−0.2987

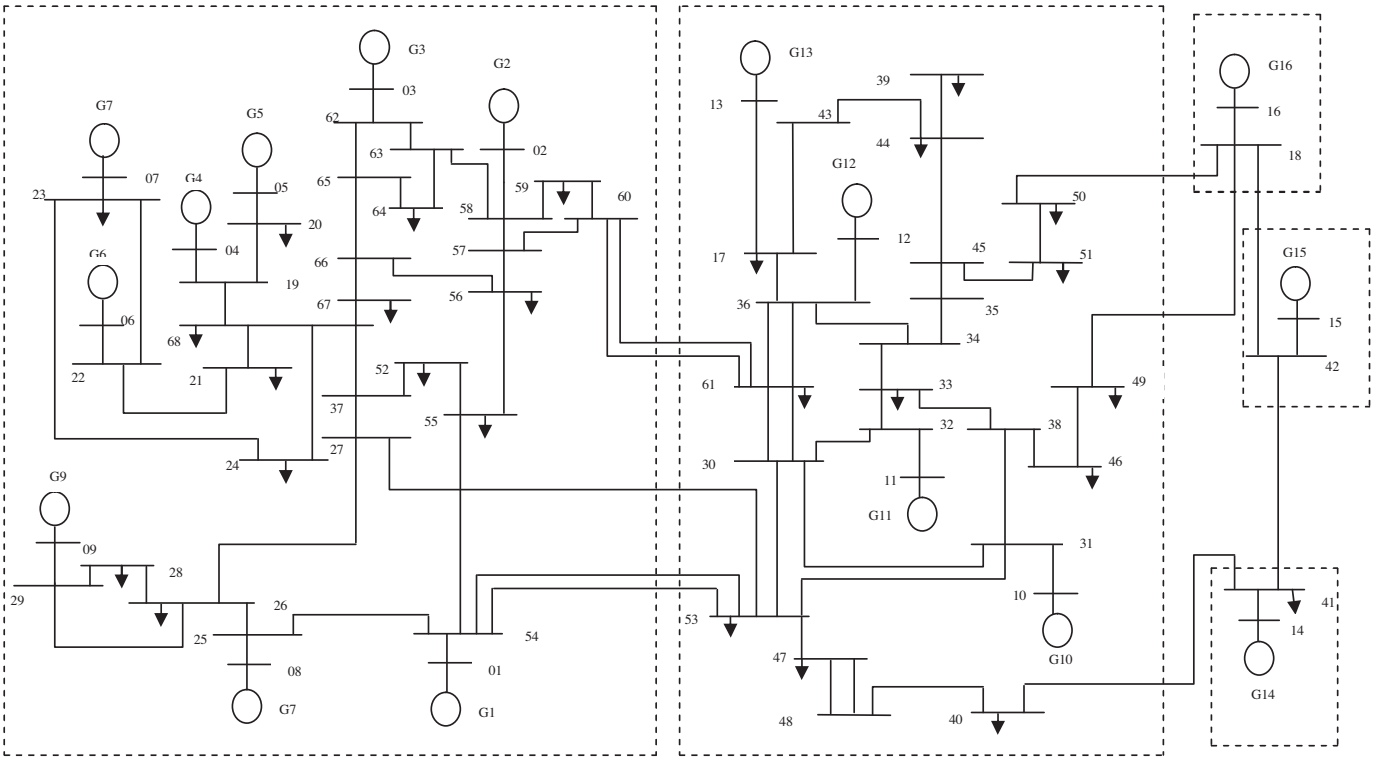

Fig. 9. IEEE 16 generator 69 bus system.

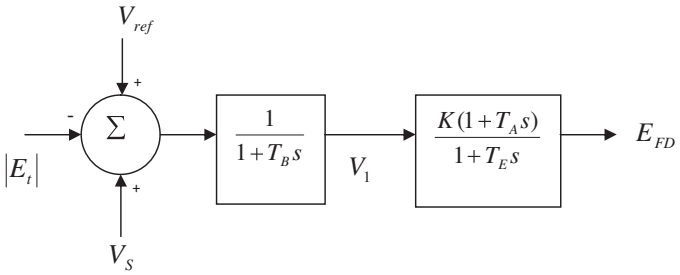

Fig. 10. Exciter model 1.

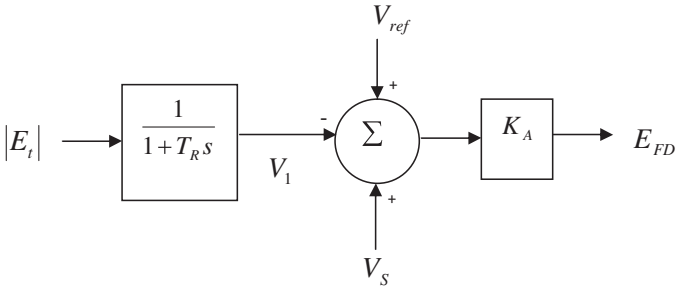

Fig. 11. Exciter model 2.

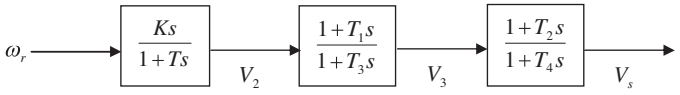

Fig. 12. Power system stabilizer model.

Table 7
Exciter model data.

Exciter model 1	K	T_A	T_B	T_E
	200	1	10	0.05
Exciter model 2	K_A		T_R	
	200		0.01	

Table 8
Power system stabilizer data.

K	T	T_1	T_2	T_3	T_4
200	10	0.05	2.97	0.02	5.4

machine model where the dynamic data are available in the pages 177–178 of [25]. All the generators were also modeled with the exciter model given in Fig. 10 with same parameters as given in Table 7 except the generator 9 which was modeled with the exciter model given in Fig. 11. Further, the generators 9, 13 and 16 were provided with the power system stabilizer model shown in Fig. 12 with the parameters as given in Table 8. In this case, the dynamic simulation was performed using PSS/E with bus 16 as an infinite bus and the reference trajectory for the exponent calculation was determined directly from PSS/E. A series of bus faults were applied and cleared after 5 cycles of the fundamental frequency. The bus faults were selected so that the post-fault system remains stable subsequent to the contingency. Largest average exponential rates of the post-fault system trajectories were calculated over a short data window where the principal axes of the hypersphere were evolved using a Jacobean matrix derived by assuming the classical generator model. Table 9 shows the results of 10 contingencies.

Table 9
Largest average exponential rates of 16 generator 69 bus system.

Faulted bus	Largest average exponential rates over different time windows				
	$(T_C)-(T_C+5)s$	$(T_C+0.5)-(T_C+5)s$	$(T_C+1.0)-(T_C+5)s$	$(T_C+1.5)-(T_C+5)s$	$(T_C+2.0)-(T_C+5)s$
17	−0.0175	0.0732	0.2828	−0.0484	−0.0883
19	0.1042	0.2039	0.2138	−0.0307	−0.0975
22	0.0326	0.0970	0.1008	−0.1103	−0.1067
31	−0.1408	−0.1419	−0.0238	−0.1916	−0.1329
32	−0.1342	−0.1377	−0.0429	−0.1583	−0.1249
36	0.0270	−0.1200	0.1815	−0.0712	−0.1074
54	−0.1586	−0.0984	0.0745	−0.0758	−0.1134
58	−0.0039	0.0036	0.0711	−0.1153	−0.1101
61	−0.0801	−0.1062	0.0391	−0.1283	−0.1225
62	−0.0481	−0.0129	0.0297	−0.1434	−0.1153

The largest average exponential rates are expected to be negative under all the scenarios as they are stable scenarios. However, it is clear that the performance of the modified algorithm has failed with the initial conditions selected at T_C, i.e. the calculations over the data window $(T_C - T_C + 5)$ s have mislead the stability conclusion under certain cases. The calculations over the $(T_C + 2) - (T_C + 5)$ s data window have accurately predicted the system stability under all the scenarios. Unstable contingencies were also generated by increasing T_C beyond the CCT and it was observed that the average largest exponential rates were all positive when the $(T_C + 2) - (T_C + 5)$ s window was used.

5. Conclusions

This paper has discussed the results of a systematic transient stability analysis performed on the power system using the concept of LEs. It has been shown that a stable post-fault power system subsequent to a given fault scenario without system topological changes can be characterized by a unique negative LLE. Furthermore, the LLE value changes with the change in the post-fault network topology. It has been found that the LLE value of the system under a specific fault scenario is invariant of the fault clearing time up to the CCT, beyond which the system becomes unstable.

The concept of LEs can be used as a theoretically sound method to determine the power system stability regions. It has been shown that it is not necessary to perform the exponent calculation until the convergence. Instead, the largest average exponential rate calculated over a short time window by selecting the initial conditions few cycles after the fault clearance provides an accurate indication of the system stability. The latter technique significantly reduces the computational burden.

References

[1] P. Kundur, Power System Stability and Control, McGraw-Hill Inc., New York, 1993.
[2] P. Kundur, J. Paserba, V. Ajjarapu, G. Andersson, A. Bose, C. Canizares, N. Hatziargyriou, D. Hill, A. Stankovic, C. Taylor, T.V. Cutsem, V. Vittal, Definition and classification of power system stability, IEEE Trans. Power Syst. 19 (2) (2004) 1387–1401.
[3] P.W. Sauer, M.A. Pai, Power System Dynamics and Stability, Prentice Hall, New Jersey, 1997.
[4] L. Wehenkel, T.V. Cutsem, M.R. Pavella, An artificial intelligence framework for on-line transient stability assessment of power systems, IEEE Power Eng. Rev. 9 (5) (1989) 77–78.
[5] L. Wehenkel, M. Pavella, E. Euxibie, B. Heilbronn, Decision tree based transient stability method a case study, IEEE Trans. Power Syst. 9 (1) (1994) 459–469.
[6] Z. Qin, J. Davidson, A.A. Fouad, Application of artificial neural networks in power system security and vulnerability assessment, IEEE Trans. Power Syst. 9 (1) (1994) 525–532.
[7] F.R. Gomez, A. Rajapakse, U.D. Annakkage, I.T. Fernando, Support vector machine-based algorithm for post-fault transient stability status prediction using synchronized measurements, IEEE Trans. Power Syst. 26 (3) (2011) 1474–1483.
[8] B. Jayasekara, U.D. Annakkage, Derivation of an accurate polynomial representation of the transient stability boundary, IEEE Trans. Power Syst. 21 (4) (2006) 1856–1863.
[9] M. Vidyasar, Nonlinear Systems Analysis, Second ed., Prentice Hall, New Jersey, 2002.
[10] F.H.J.R. Silva, L.F.C. Alberto, N.G. Bretas, Extended Lyapunov functions for power systems with transmission losses, Proc. of IEEE Bologna Power Tech conf. 3, 2003.
[11] R.J. Davy, I.A. Hiskens, Lyapunov functions for multimachine power systems with dynamic loads, IEEE Trans. Circ. Syst. 1: Fund. Theor. Appl. 44 (9) (1997) 796–812.
[12] H. Kwatny, L. Bahar, A. Pasrija, Energy-like Lyapunov functions for power systems stability analysis, IEEE Trans. Circ. Syst. 32 (11) (1985) 1140–1149.
[13] H.R. Pota, P.J. Moylan, A new Lyapunov functions for interconnected power systems, IEEE Trans. Automatic Control 37 (8) (1992) 1192–1196.
[14] A. Wolf, J.B. Swift, H.L. Swinney, J.A. Vastano, Determining Lyapunov exponents from a time series, Phys. D 16 (1985) 285–317.
[15] W. Kinsner, Characterizing chaos through Lyapunov metrics, IEEE Trans. Syst. Man Cybern. – Part C: Appl. Rev. 36 (2) (2006) 141–151.
[16] E. Ott, Chaos in Dynamical Systems, Second ed., Cambridge University Press, New York, 2002.
[17] C. Liu, J.S. Thorp, J. Lu, R.J. Thomas, H. Chiang, Detection of transiently chaotic swings in power systems using real-time phasor measurements, IEEE Trans. Power Syst. 9 (3) (1994) 1285–1292.
[18] J. Yan, C.C. Liu, U. Vaidya, PMU-based monitoring of rotor dynamics, IEEE Trans. Power Syst. 26 (4) (2011) 2125–2133.
[19] W. Suampun, H.D. Chiang, Critical evaluation of methods for estimating stability boundary for transient stability analysis in power system, PES Gen. Meet. (2010) 1–8.
[20] I. Genc, R. Diao, V. Vittal, S. Kolluri, S. Mandal, Decision-tree based preventive and corrective control applications for dynamic security enhancement in power systems, IEEE Trans. Power Syst. 25 (3) (2010) 1611–1619.
[21] Power Tec Lab, BC, Canada, Transient Security Assessment Tool (TSAT)–User Man., April 2009.
[22] V.I. Oseledec, A multiplicative ergodic theorem: Lyapunov characteristic numbers for dynamical system, Trans. Mosc. Math. Soc. 19 (1968) 197–231.
[23] A. Dabrowski, Estimation of the largest Lyapunov exponent from the perturbation vector and its derivative dot product, Nonlinear Dyn. 67 (2012) 283–291.
[24] K. Ramasubramanian, M.S. Sriram, A comparative study of computation of Lyapunov spectra with different algorithms, Phys. D 139 (2000) 72–86.
[25] B. Chaudhuri, B. Pal, Robust Control in Power Systems, Springer, New York, 2005.